



Efficient evolution framework for chirality control in non-Hermitian systems with adiabaticity engineering

Dong Wang,^{1,2,3,4,*} Wen-Xi Huang,^{5,*} Bo Zhou,^{1,2,3,4} Wenduo Yu,^{1,2,3,4} Pei-Chao Cao ^{1,2,3,4} Yu-Gui Peng,⁵ Zheng-Yang Zhou,⁶ Hongsheng Chen,^{1,2,3,4,†} Xue-Feng Zhu,^{5,‡} and Ying Li ^{1,2,3,4,§}

¹State Key Laboratory of Extreme Photonics and Instrumentation, Key Laboratory of Advanced Micro/Nano Electronic Devices & Smart Systems of Zhejiang, Zhejiang University, Hangzhou 310027, China

²International Joint Innovation Center, The Electromagnetics Academy at Zhejiang University, Zhejiang University, Haining 314400, China

³Jinhua Institute of Zhejiang University, Zhejiang University, Jinhua 321099, China

⁴Shaoxing Institute of Zhejiang University, Zhejiang University, Shaoxing 312000, China

⁵School of Physics and Innovation Institute, Huazhong University of Science and Technology, Wuhan 430074, China

⁶Key Laboratory of Optical Field Manipulation of Zhejiang Province, Department of Physics, Zhejiang Sci-Tech University, Hangzhou 310018, China



(Received 20 June 2023; revised 4 July 2024; accepted 11 July 2024; published 12 August 2024)

The eigenvalue of a non-Hermitian Hamiltonian often forms a self-intersecting Riemann surface, leading to a unique mode conversion phenomenon when the Hamiltonian evolves along certain loop paths around an exceptional point (EP). However, two fundamental problems exist with the conventional scheme of EP encircling: the speed of mode conversion is restricted by the adiabatic requirement, and the chirality cannot be freely controlled. Here, we introduce a method which dynamically engineers the adiabaticity in the evolution of non-Hermitian Hamiltonians that allows for both chiral and nonchiral mode conversion on the same path. Our method is based on quantifying and controlling the instantaneous adiabaticity, allowing for nonuniform evolution throughout the entire path. We apply our method into the microwave waveguide system and by optimizing the distributed adiabaticity along the evolution loop, we achieve the same quality of mode conversion as conventional quasiadiabatic evolution in only one-fourth of the time. Our approach provides an on-demand solution to address the speed and chirality challenges associated with EP encircling, which does not depend on specific model. It also facilitates the dynamic manipulation and regulation of nonadiabatic processes, thereby accelerating the operation and allowing for a selection among various mode conversion patterns.

DOI: [10.1103/PhysRevB.110.064308](https://doi.org/10.1103/PhysRevB.110.064308)

I. INTRODUCTION

Non-Hermitian systems can exhibit exceptional points (EPs) where eigenvalues and eigenstates coalesce [1–4]. EPs have been extensively studied for their unique properties in the field of photonics [5–9], acoustics [10–14], and beyond [15], which can be implemented for single-mode lasing [16,17], loss-induced transmission enhancement [18], and unidirectional invisibility [19,20]. The eigenvalues of these non-Hermitian Hamiltonians form a self-intersecting Riemann surface, causing the initial eigenstate to be irrecoverable after completing a loop around an EP [21]. Mode conversion can be achieved by adiabatically encircling an EP, but only in one direction (e.g., counterclockwise, CCW) [22]. In the opposite direction (e.g., clockwise, CW), the Hamiltonian transitions to a lower imaginary Riemann sheet, leading to a nonadiabatic jump and subsequent recovery of the initial state [23–32]. This asymmetric mode conversion highlights the chirality of EP encircling and has sparked significant

research interest, particularly in applications such as optical communications [30], quantum control [31], and optical isolators [32].

Despite notable progress, the EP encircling scheme faces two fundamental problems. Firstly, the adiabatic requirement limits mode conversion speed, impacting operational efficiency and mode decay. Recent approaches, like Hamiltonian hopping [33] and selected loops [29], aim to accelerate evolution but are hindered by extreme parameters and low-loss eigenstates, restricting broader applicability. Secondly, controlling chirality in mode conversion is constrained. Conventional schemes permit only chiral mode conversion (mode $A \rightarrow B$ in CCW, mode $A \rightarrow A$ in CW). Recent findings shows potential for nonchiral mode recovery (mode $A \rightarrow A$ in CCW and CW) via a nonencircling-EP loop path [34], however, the specific outcome depends on the path details. And nonchiral mode conversion (mode $A \rightarrow B$ in CW and CCW) remains insufficiently explored, reportedly achievable only with specific starting points in the evolution process [28]. Addressing speed and chirality challenges in EP encircling requires an efficient and model-independent solution, as existing works rely on specific models, paths, or Hamiltonians, necessitating broader approaches. Adiabaticity offers potential solutions but lacks adequate exploration. Existing schemes focus on maintaining proximity to the Riemann surface throughout the encircling

*These authors contributed equally to this work.

†Contact author: hansomchen@zju.edu.cn

‡Contact author: xfzhu@hust.edu.cn

§Contact author: eleying@zju.edu.cn

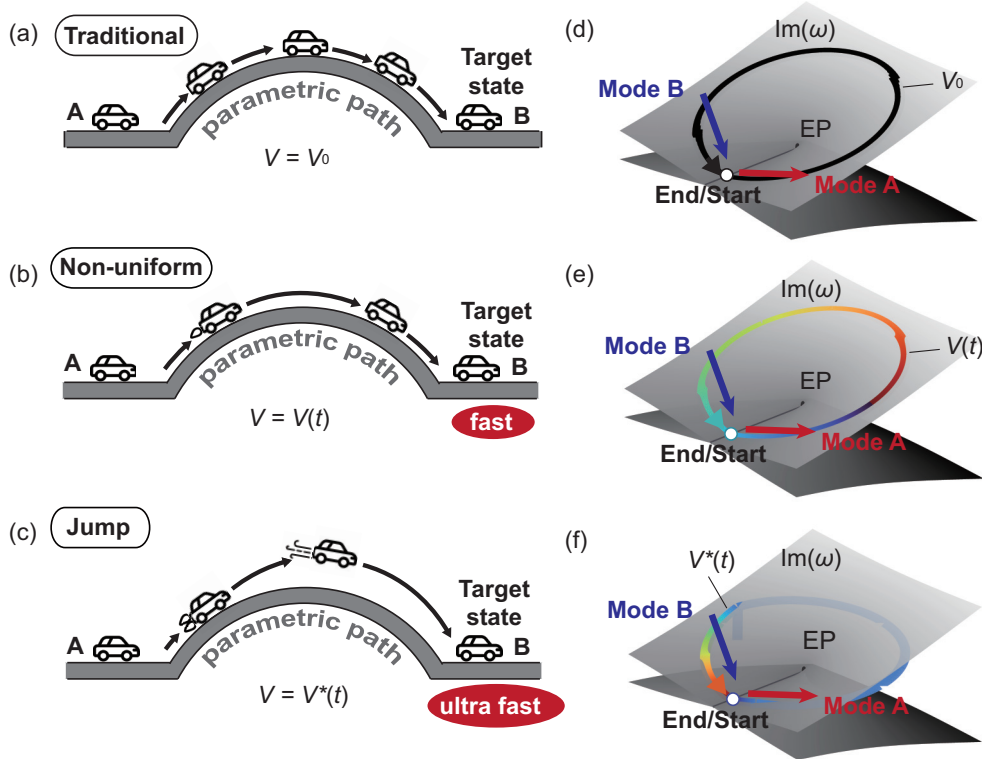


FIG. 1. The schematic diagram of fast mode conversion through adiabatic engineering along the parameter path. (a) Adiabaticity maintains system on arch bridge surface, limiting velocity for uniform evolution. (b) Nonuniform speed function $v(t)$ designed by considering speed limitations to accelerate evolution. (c) Adiabatic restrictions relaxed at certain points for faster evolution toward target state. (d), (e), (f) The corresponding cases on Riemann surface show counterclockwise evolution from branch cut, looping EP, returning to initial point, transitioning Modes A to B. Lines depict system's parameter space position and evolution speed variation. (d) Uniform speed v_0 , (e) Nonuniform speed $v(t)$ determined by adiabaticity at each point, (f) The “jump” evolution deviating from Riemann surface at certain points.

operation, with occasional jumps, yet fail to consider the degree of adiabaticity at each instant. A systematic method to quantify and control instantaneous adiabaticity is currently absent, impeding efficiency optimization. Furthermore, nonadiabaticity engineering has been overlooked, with previous approaches either avoiding nonadiabatic processes in mode conversion or limiting nonadiabatic jumps between Riemann sheets in mode recovery. The active introduction and control of nonadiabatic processes remain rare, limiting the ability to accelerate operations and freely select mode conversion patterns. Overall, an on-demand approach addressing the speed and chirality challenges in EP encircling is urgently needed, with adiabaticity playing a crucial role that requires further attention.

We introduce dynamic adiabaticity engineering for non-Hermitian Hamiltonian evolution, achieving equivalent quality to conventional quasiadiabatic evolution in one-fourth of the time. Our method facilitates both chiral and nonchiral mode conversions on a single path. By optimizing velocity at each local point based on quantified adiabaticity, we transcend the adiabatic/nonadiabatic dichotomy, integrating both processes within a unified framework. Importantly, our methodology allows deviation from the Riemann surface, offering an alternative to strict adherence or jumps between surfaces. Implemented in a microwave waveguide system, our approach demonstrates superior speed and mode purity. Moreover, it extends beyond optical systems, be-

ing applicable to various non-Hermitian systems. Our work enhances understanding of adiabaticity in non-Hermitian systems and provides insights for advancing mode converters. The dynamic adiabaticity engineering method is a promising approach for achieving efficient and high-quality evolution in non-Hermitian systems.

II. ADIABATICITY ENGINEERING

In the study of general chiral phenomena, to achieve mode conversion, the state necessitates evolving while adhering to the upper imaginary Riemann surface. This is typically accomplished by evolving slowly along a parameter path. To quantify this speed, we introduce a function $C(x)$ to represent the position of a N -level system on a certain parameter path: $dC^2(x) = \sum_1^N dx_n^2/\rho$, $\int_C dC = 1$, where ρ is the normalization factor. Thus, the parameter change speed is $v = dC/dt$. In most cases, the system moves at a constant speed v_0 (slow enough), as illustrated in Fig. 1(a). However, uniform evolution is not optimal due to inconsistent adiabaticity. This inconsistency can be visualized with the parameter path as an arch bridge, where positions have varying “escape velocities”, indicating adiabaticity. Adiabatic evolution requires the system to stay on the bridge surface.

A nonuniform evolution speed $v(t)$ can be designed based on the adiabatic requirement along the path: high adiabaticity demands low speed, while low adiabaticity demands high

speed, expediting mode conversion [Fig. 1(b)]. It appears this adiabaticity-dependent evolution scheme is fastest if adiabaticity must be preserved throughout the evolution path. However, practical scenarios require rapid evolution to a steady state, such as stochastic heat engines [35] and genotype probability distribution in a population [36]. When mode conversion effect is the focus, the process can be faster if abandoning adiabaticity of a certain path, causing the “jump” evolution [Fig. 1(c)]. Physically, these three different forms of evolution are represented on the Riemann surface, as qualitatively depicted in Figs. 1(d) and 1(e). The evolution speed $v^*(t)$ in jump evolution is anomalous:

$$v^*(t) = \begin{cases} \delta(t), & \text{for positions the dwell time is zero} \\ v(t), & \text{for positions the dwell time is nonzero} \end{cases} \quad (1)$$

where $\delta(t)$ is Dirac delta function.

Different positions along the parameter path have varying adiabaticity requirements, requiring quantification before investigating the newly proposed dynamic evolution methods. In our study, system's state during evolution is approximately obtained through difference iteration after discretization:

$$|\Psi_j\rangle = \sum_n c_{n,j} |\psi_{n,j}\rangle, \quad (2)$$

$$|\Psi_{j+1}\rangle = \sum_n \langle \theta_{n,j+1} | \Psi_j \rangle e^{-i\omega_{n,j+1} \Delta t_j} |\psi_{n,j+1}\rangle. \quad (3)$$

Here, $\{\langle \theta_n | \}$ and $\{|\psi_n\rangle\}$ are the normalized biorthogonal basis of the non-Hermitian Hamiltonian. The subscript n is sorted from the largest to the smallest according to the imaginary part of the eigenvalue. The subscript j represents the j th parameter point, Δt_j is the evolving time at the j th parameter point, $c_{n,j}$ is the coefficient of eigenstate $|\psi_{n,j}\rangle$, $\omega_{n,j+1}$ is the corresponding eigenvalue of eigenstate $|\psi_{n,j+1}\rangle$, and $\langle \theta_{n,j+1} | \Psi_j \rangle e^{-i\omega_{n,j+1} \Delta t_j}$ actually stands for $c_{n,j+1}$. We use a weighted eigenvalue $\bar{\omega}_j$ to characterize the system's state on the Riemann surface:

$$\bar{\omega}_j = \sum_n \frac{|c_{n,j}|^2}{\sum_m |c_{m,j}|^2} \omega_{n,j}. \quad (4)$$

Next, we define the proportion $P_{n,j}$ of the instantaneous eigenstate $|\psi_{n,j}\rangle$ as $P_{n,j} = |c_{n,j}|^2 / \sum_m |c_{m,j}|^2$. Adiabatic evolution requires the system to predominantly occupy the least decaying state, meaning $P_{1,j}$, representing instantaneous eigenstates with the largest imaginary parts, should not fall below a specific value denoted as $P_{1,j} \geq P_0$. A higher P_0 signifies increased adiabaticity. Varying P_0 allows for different evolutionary configurations based on distinct adiabatic requirements. If $P_{1,j} < P_0$, it requires increasing the evolving time Δt_j (reducing evolving speed) at the j th parameter point to enhance adiabaticity. Conversely, if $P_{1,j} > P_0$, it permits reducing evolving time (increasing evolving speed) or even skipping the parameter point until P_1 fall into P_0 . Note that P_0 must be less than 1, as changing system parameters cause coefficients of the instantaneous eigenstates to change, making complete adiabaticity unattainable.

III. STABLE CONVERSION

By setting P_0 at a constant value and ensuring $P_{1,j} = P_0$, we can achieve maximum velocity while maintaining high purity of the final state under this adiabaticity constraint. This strategy, termed “stable conversion configuration”, dynamically adjusts the dominant proportion to uphold the final state's purity. The residence time Δt_j at each parameter point along the evolution path is calculated as follows: Give the current state $|\Psi_j\rangle$, the dominant state proportion at the next parameter point is determined by the equation:

$$P_{1,j+1} = \frac{|\langle \theta_{1,j+1} | \Psi_j \rangle e^{-i\omega_{1,j+1} \Delta t_j}|^2}{\sum_n |\langle \theta_{n,j+1} | \Psi_j \rangle e^{-i\omega_{n,j+1} \Delta t_j}|^2}. \quad (5)$$

Letting $P_{1,j+1}$ be equal to P_0 to satisfy the adiabatic evolution requirement simplifies the equation to a single-variable form with Δt_j as the variable. Solving this equation yields the residence time Δt_j for each parameter point, thereby obtaining the set of evolution times $\{\Delta t_j\}$ [see Note 2 in the Supplemental Material (SM)] [37].

In this study, we consider a non-Hermitian system with EP:

$$\hat{H} = \begin{pmatrix} x + iy & 1 \\ 1 & -x - iy \end{pmatrix}. \quad (6)$$

The Hamiltonian of most two-level systems with equal coupling, $\hat{H}_a = \begin{pmatrix} a + ib & e \\ e & c + id \end{pmatrix}$, can be transformed into this form (see Note 5 in the SM [37]). Here $x, y, a, b, c, d \in \mathbb{R}$ and $e \in \mathbb{C}$. Since the Hamiltonian in Eq. (6) does not involve a specific model, we could define the evolution time of Eq. (6) as normalized time, by dividing the actual time by the characteristic time of the system, with the coupling coefficient e being selected as the characteristic time here: $t_{\text{norm}} = t/e$.

The results of stable conversion configuration (nonuniform evolution) are presented in Fig. 2, showcasing the evolution time set $\{\Delta t_j\}$ and trajectory in Figs. 2(a) and 2(b). The parameter path comprises 100 equal intervals, totaling 101 parameter points. Initially, $P_{1,j=0} = 1$, reflecting the input state $|\psi_{1,j=0}\rangle$ and $|\Psi_0\rangle = |\psi_{1,j=0}\rangle$. This evolutionary path can be bypassed until $P_{1,j}$ decreases to the value of P_0 . In this configuration, we examined two input modes and directions [Figs. 2(c) and 2(f)], where $\zeta_{A,B}$ represents the coefficient of Mode A or Mode B: $\zeta_{A,B;j} = |\langle \theta_{A,B} | \Psi_j \rangle|^2 / \sum_{A,B} |\langle \theta_{A,B} | \Psi_j \rangle|^2$. Mode A and Mode B correspond to the system's two eigenstates on the imaginary part branch cut where the eigenvalues ω_1 and ω_2 from Eq. (6) satisfy $\text{Im}(\omega_1) = \text{Im}(\omega_2)$, namely $|\psi_A\rangle = |\psi_{1,j=0}\rangle$ and $|\psi_B\rangle = |\psi_{2,j=0}\rangle$. For comparison, the conventional uniform evolution is calculated in Figs. 2(c)–2(f). There are two approaches to comparing the efficiency of these evolution methods. One approach is to compare the time required to achieve the same final state purity. The other approach is to compare the final state purity achieved within the same time frame. In Figs. 2(c)–2(f), we presented the result of the second approach. For the first approach, the results are given in Figs. 3(h) and 4(f). The time required for uniform evolution to achieve mode conversion is 5.05 normalized time, and to achieve mode recovery is 4.53 normalized time (see Fig. S8 in the Supplemental Material).

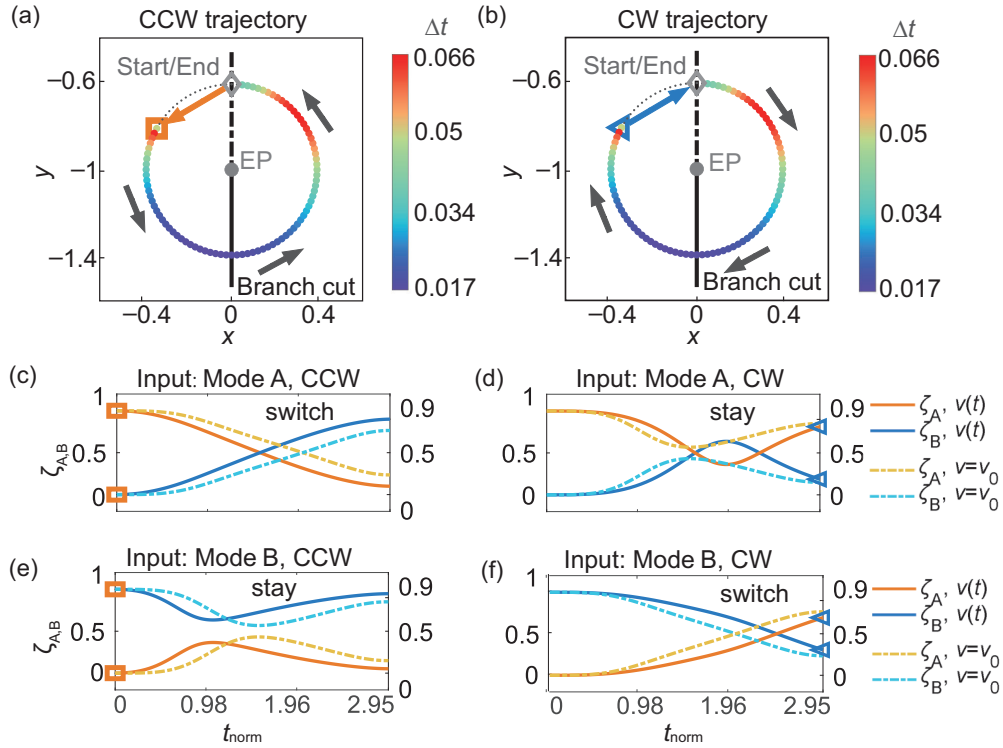


FIG. 2. Bimodal chiral mode conversion in nonuniform evolution. (a), (b) show evolution time set $\{\Delta t_j\}$, patterns, and evolution trajectories (CCW and CW cases) for chiral cases in x - y parameter planes. The branch cuts where $\text{Re}(\omega_1) = \text{Re}(\omega_2)$ and $\text{Im}(\omega_1) = \text{Im}(\omega_2)$ are shown by solid and dashed lines, respectively. $P_0 = 0.9$. Gray rhombus denotes start/end point. (c)–(f) depict chiral mode conversion effect for Mode A and B. Mode A switches to B in CCW, remains A in CW; Mode B remains B in CCW, switches to A in CW. Orange box and blue triangle mark start and end of the actual evolved portion along parameter path. The case of uniform evolution (dashed line) is included for comparison. Here, we assess the efficiency of uniform versus nonuniform evolution by comparing the final state purity achieved within the same time. The higher the final state purity within the same duration, the faster the evolution is.

Both modes exhibit chiral mode conversion effects. Faster and more pure mode conversion is achieved for Mode A [Fig. 2(c)]. However, the transfer effect is suboptimal for Mode B [Fig. 2(e)] due to the skipped parameter path at the beginning of CCW evolution, which becomes the last path of CW evolution while the evolution time set $\{\Delta t_j\}$ is based on CCW evolution. Additional constraints are required to optimize the effectiveness of CW dynamic evolution. The stable conversion configuration optimizes the conventional method, with the underlying physics rooted in the concept of “nonadiabatic jump” as postulated in conventional chiral conversion. Consequently, the framework does not allow for achieving the nonchiral effect demonstrated in the section *Swift nonchiral mode conversion*.

IV. DEMAND-DRIVEN STRATEGY FOR DYNAMICAL EVOLUTION

The parameter variations in a time-varying system are accompanied by changes in the instantaneous eigenvectors. The instantaneous eigenvector $\psi_1(t)$ at one parameter position will decompose orthogonally into components of $\psi_2(t)$ at the next parameter position and add to the corresponding instantaneous eigenstate, thus altering its amplitude. The same applies to $\psi_2(t)$. The coefficients of these components are complex numbers with phases that vary over time and are

coupled with each other, making their impact on amplitude changes difficult to predict theoretically. Since the coefficients in this process evolve in a coupled manner and cannot be optimized using conventional methods, employing computational algorithms becomes a more viable option. Utilizing the stable conversion configuration yields two conditions during evolution: I. Instantaneous jumps between parameter points, and II. Static evolution at a specific parameter point for Δt_j . While Procedure I may overlook adiabaticity along certain evolution paths, Procedure II compensates. Optimal results of dynamic evolution, tailored to specific requirements, depend on the appropriate combination of jump and static evolution points using the evolution time set $\{\Delta t_j\}$. Thus, all dynamic evolution problems can be formulated as optimization problems within our framework, differing only in imposed constraints: I. Enclosed parameter path; II. Evolutionary direction (CCW or CW); III. Input mode; IV. Desired end state and its purity. Optimizing a time-dependent Hamiltonian to convert between desired modes is a broad and long-studies field [38]. In the realm of optimizing the evolution of quantum states, quantum optimal control theory stands as a highly efficacious approach [39–41]. However, it is primarily employed for optimizing evolutionary path [40]. While in our optimization problem, the evolution path is fixed. The purpose of this constraint is to eliminate other interfering factors so that we can focus on the effect of adiabaticity adjustment itself. This strong constraint

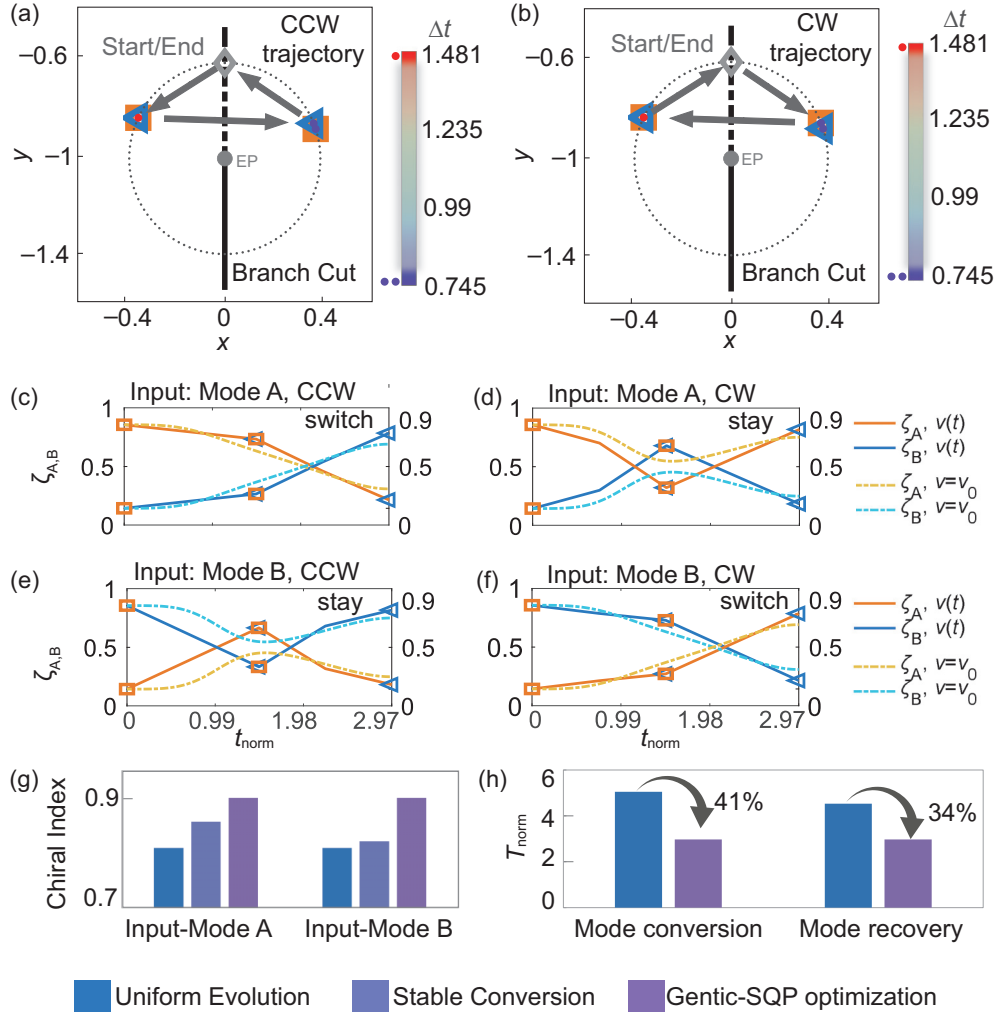


FIG. 3. Bimodal chiral mode conversion via genetic-SQP optimization. (a), (b) display evolution time set $\{\Delta t_j\}$ and patterns in CCW and CW parameter planes. The algorithm selects only three parameter points for evolution, skipping a substantial portion of path (red and blue dots). (c)–(f) illustrate the chiral mode conversion for Mode A and B. (g) compares chiral effects achieved through uniform evolution, stable conversion, and genetic-SQP optimization. Optimized evolution demonstrates advantages in speed, end state purity, chiral effect, and robustness (chiral effect being independent of input mode). (h) compares time required to achieve 90% end state in mode conversion and mode recovery. The time is reduced 41% and 34% for mode conversion and mode recovery, respectively.

reduces the searching space in the optimization process. Therefore, we choose conventional optimization algorithms which are already capable of determining the optimal solution. It is possible to further improve efficiency or solve more complex problems if the quantum optimal control theory is used. This, however, is beyond the scope of this study. Here, we adopt combined approach utilizing the genetic algorithm [42] and the Sequential Quadratic Programming (SQP) algorithm [43]. For a comprehensive algorithmic description, refer to Note 3 in the SM [37].

V. SWIFT BIMODAL CHIRAL EVOLUTION

To demonstrate the superiority of our algorithm, we performed bimodal chiral evolution and presented the results in Figs. 3(e) and 3(f). The evolution processes of CCW and CW directions in the parameter plane are depicted in Figs. 3(a) and 3(b). Notably, the optimized path enables the system

to bypass most regions of the evolutionary path and remain at specific parameter points. These parameter jumps occur instantaneously without altering the state in the representation of Mode A/B. The mode-switching and mode-recovery phenomena arise from static evolution at these characteristic points, compensating for adiabaticity. By incorporating these jumps and stagnation, the adiabaticity is modulated, resulting in a substantial reduction in evolution time. Comparing the outcomes with uniform evolution, we observe faster mode-conversion or mode-recovery effects [Fig. 3(h)] and higher purity of the end states in all four cases, validating our assumption. It is important to note that these “perfect” results are achieved through the constraints established within our evolution framework (for further details, see Note 4 in the Supplemental Material). In Figs. 3(a) and 3(b), it is shown that the trajectory generated by the proposed algorithm does not enclose the EP. This outcome arises from the algorithm optimizing the dwell time at different parameter points along

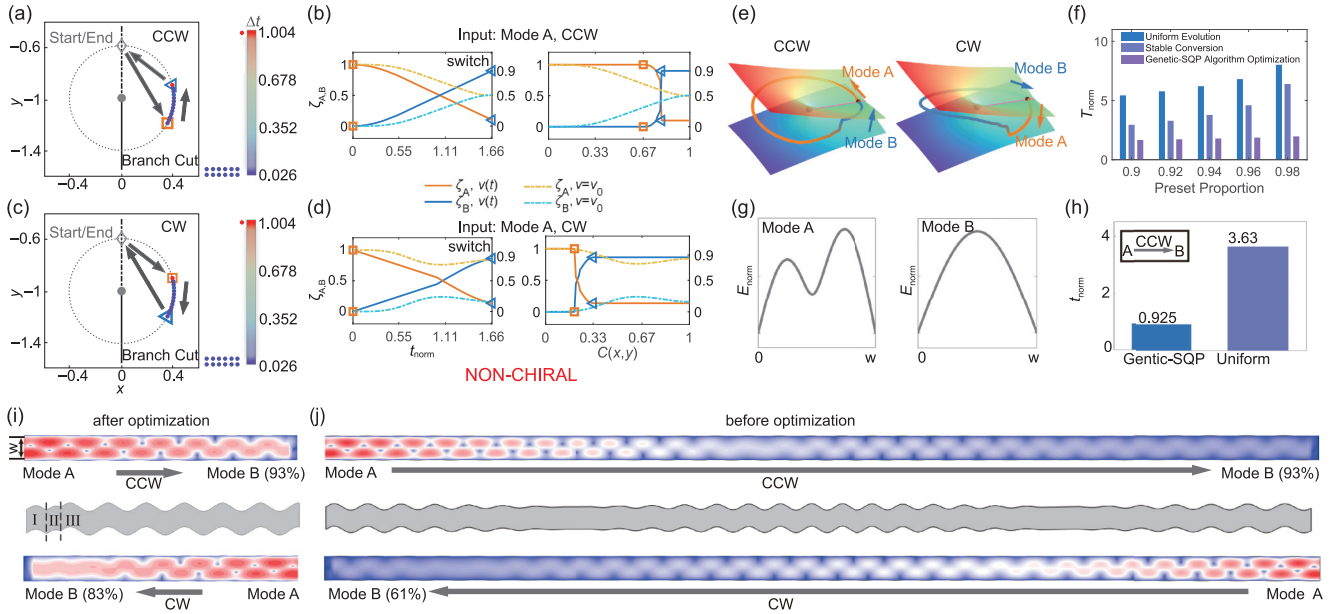


FIG. 4. Swift nonchiral mode conversion via genetic-SQP optimization. (a), (c) depict evolution time set $\{\Delta t_j\}$ for nonchiral cases and patterns in CCW and CW parameter planes. The algorithm selects a specific path portion (red and blue dots). (b), (d) showcase nonchiral state evolution effect for Mode A. (e) display the change in weighted eigenvalue $\text{Im}(\bar{\omega})$ of system's state on the Riemann surfaces for CCW and CW with respect to Mode A. Orange region: Mode A dominance; blue: Mode B dominance. (f) compares time consumption of three evolution methods for different final state purity requirements. (i), (j) Geometry and effects before and after optimization. The middle subfigures are the geometries of waveguide, where the boundary amplitude σ is magnified ($\times 20$) for visibility. (h) Time consumption (waveguide length) for optimized and conventional waveguide to realize mode conversion in CCW evolution. (g) Normalized electric field of Mode A and B.

a circular path around the EP. Since the optimized dwell time at most parameter points is zero, the resulting trajectory does not enclose the EP. Consequently, within our framework, the concept of encircling the EP becomes less significant, as the focus shifts to the geometric properties of the system's Riemann surface. Even for a loop that theoretically encircles the EP, our method may select an optimized trajectory that does not actually enclose the EP. It is consistent with previous work realizing chiral effect without encircling an EP [34,44].

We introduced the chiral index (CI) as a metric to evaluate the quality of the chiral mode conversion effect. The CI is calculated as the average of $\zeta_{A,B}$ for end states in CCW and CW: $\text{CI} = \frac{1}{2} \max\{(\zeta_{A;\text{end}}, \zeta_{B;\text{end}})|\text{CCW}\} + \frac{1}{2} \max\{(\zeta_{A;\text{end}}, \zeta_{B;\text{end}})|\text{CW}\}$. A higher CI indicates a stronger chirality in the process. The chiral effects of uniform evolution, stable conversion configuration, and genetic-SQP algorithm optimization for different input modes are illustrated in Fig. 3(g). Both the stable conversion and genetic-SQP methods demonstrate superior chiral effects compared to uniform evolution. Moreover, the genetic-SQP method offers an advantage over the stable conversion method as it is independent of the input mode, providing greater potential for practical chiral converters.

VI. SWIFT NONCHIRAL MODE CONVERSION

The stable and fast dynamic evolution configuration framework introduced earlier has demonstrated rapid transitions, high purity, and remarkable chiral index in chiral mode conversion effects. It should be pointed out that our method is a demand-orientated framework designed for dynamic evolu-

tion near EP. Beyond chiral evolution, our approach can be extended to achieve various other dynamic evolution effects, including nonchiral evolution, by incorporating corresponding constraints into the optimization process.

Through adjustments in the imposed constraints (see Note 4 in the SM [37]), we achieved nonchiral evolution and obtained faster mode conversion processes, as depicted in Fig. 4. In this context, ‘‘chiral’’ refers to the distinct phenomena evolving in CCW and CW directions, while nonchiral evolution indicates identical output modes, regardless of the evolution direction. For Mode A, we successfully realized the mode conversion effect in both CCW [Fig. 4(b)] and CW evolution [Fig. 4(d)], corresponding to the previously mentioned nonchiral mode conversion. Notably, our configuration achieved rapid mode conversion using only a small portion of the parameter path [Fig. 4(a)], attributed to the significant variation in $\text{Im}(\bar{\omega})$ values along this segment, leading to fast changes in the distribution of instantaneous eigenstates. Therefore, the algorithm concentrated the evolution in this region. In addition to the effect of variation in $\text{Im}(\bar{\omega})$, the projection of instantaneous eigenstates is another vital contributor for algorithm's decision-making process (see Note 7 in the Supplemental Material). The evolutionary behavior is also observed in the imaginary Riemann surfaces [Fig. 4(e)], indicating the delicate balance between freeing adiabaticity and maintaining the state's purity along the path. We observed fluctuations in $\text{Im}(\bar{\omega})$ on the skipped parameter path even if the system did not evolve in certain parameters, due to the variation in the instantaneous eigenvectors. In contrast, on the parameter path where the system remains, $\text{Im}(\bar{\omega})$ increases.

To highlight the advantages of our approach in term of time consumption, we compare the evolution time required to achieve different final state switching proportions using three methods: Uniform evolution, Stable conversion, and genetic-SQP algorithm optimization under varying final state purity requirements. The results are shown in Fig. 4(f). It is evident that the genetic-SQP algorithm optimization method exhibits significantly reduced time consumption compared to the first two methods. Furthermore, the growth in time consumption is not substantial as the final state purity constraint changes. The advantage of the genetic-SQP method becomes more pronounced with higher requirements for final purity.

VII. MICROWAVE WAVEGUIDE SYSTEM

To validate our approach in real-world applications, we implement it in a well-known microwave waveguide system as a case study [23]. As a periodic waveguide, the waveguide boundary amplitude σ and boundary wavenumber detuning δ serve as our modulation parameters. Its details and modulation are presented in the Supplemental Material. We simplified constraints to only focus on Mode A converting into Mode B in both the CCW and CW directions. (in a waveguide, CCW evolution means field transmits from left to right and CW evolution, from right to left). Mode A and B are two eigenmodes of the periodic waveguide at starting parameter point. Before optimization, the variables δ and σ changes continuously and satisfy $\delta = \delta_{EP} + \delta_r \cos(\theta + \pi/2)$, $\sigma = \sigma_{EP} + \sigma_r \sin(\theta + \pi/2)$ for $\theta \in [0, 2\pi]$. After optimization, the algorithm selects three parameters in the parameter path of conventional scheme to evolve [part I, II, and III in Fig. 4(i)], which are (δ_1, σ_1) for $\Delta t_{norm1} = 0.068$, (δ_2, σ_2) for $\Delta t_{norm2} = 0.047$, (δ_3, σ_3) for $\Delta t_{norm3} = 0.810$. The total normalized time required to achieve nonchiral mode conversion after optimization is $\Delta t_{after} = 0.925$, while $\Delta t_{before} = 3.63$. The specific values of the model are included in the Note 6 of Supplemental Material. The results, depicted in Figs. 4(h)–4(j), reveal a significant reduction in time (length) compared to conventional methods in mode conversion. Moreover, our method demonstrates superior performance in CW evolution,

with Mode B constituting 83% in the optimized waveguide versus 61% in the conventional one, indicating its superiority. Our method extends beyond waveguide systems, applying to diverse nonHermitian systems characterized by nontrivial geometric properties on Riemann surfaces and also to cavity networks with time-varying coupling improved transient logic operation response [45]. Furthermore, the optimization objective can be tailored accordingly. While our study focuses on optimizing time, other scenarios, such as quantum heat engine [46], may prioritize efficiency, defined as the ratio of net work output to energy input, as the optimization target function.

VIII. CONCLUSION

We have demonstrated that strict adherence to adiabaticity throughout the parameter loop is not always necessary in the dynamic evolution of non-Hermitian systems, especially when prioritizing mode conversion results or chiral effects. Building upon this insight, we have presented an on-demand and model-independent method capable of realizing both chiral and nonchiral phenomena while accommodating any desired purity requirement for the final state. In contrast to traditional encircling approaches, our analytical and computational configuration offers notable advantages, including enhanced speed, model independence, and the ability to generate novel effects. These findings contribute to a deeper understanding of non-Hermitian dynamic evolution. Moreover, the potential application of our method is broad, besides the example demonstration in waveguide system, any N-level systems can make use of this method to optimize computational resources, modulation of intermediate process quantity, and result reconfiguration.

ACKNOWLEDGMENTS

This work is supported by the National Key R&D Program of China under Grant No. 2022YFA1405200, the National Natural Science Foundation of China (NNSFC) under Grants No. 92163123 and No. 52250191, the Zhejiang Provincial Natural Science Foundation of China under Grant No. LZ24A050002.

-
- [1] T. Kato, *Perturbation Theory for Linear Operators* (Springer, New York, 1966).
 - [2] Y. Ashida, Z. Gong, and M. Ueda, Non-Hermitian physics, *Adv. Phys.* **69**, 249 (2020).
 - [3] K. Kawabata, K. Shiozaki, M. Ueda, and M. Sato, Symmetry and topology in non-Hermitian physics, *Phys. Rev. X* **9**, 041015 (2019).
 - [4] K. Ding, G. Ma, M. Xiao, Z. Q. Zhang, and C. T. Chan, Emergence, coalescence, and topological properties of multiple exceptional points and their experimental realization, *Phys. Rev. X* **6**, 021007 (2016).
 - [5] R. El-Ganainy, K. G. Makris, M. Khajavikhan, Z. H. Musslimani, S. Rotter, and D. N. Christodoulides, Non-Hermitian physics and PT symmetry, *Nat. Phys.* **14**, 11 (2018).
 - [6] L. Feng, R. El-Ganainy, and L. Ge, Non-Hermitian photonics based on parity–time symmetry, *Nat. Photonics* **11**, 752 (2017).
 - [7] Ş. K. Özdemir, S. Rotter, F. Nori, and L. Yang, Parity–time symmetry and exceptional points in photonics, *Nat. Mater.* **18**, 783 (2019).
 - [8] Z. Chen and M. Segev, Highlighting photonics: Looking into the next decade, *ELight* **1**, 2 (2021).
 - [9] X. Mao, G.-Q. Qin, H. Zhang, B.-Y. Wang, D. Long, G.-Q. Li, and G.-L. Long, Enhanced sensing mechanism based on shifting an exceptional point, *Research* **6**, 0260 (2023).
 - [10] X.-F. Zhu, H. Ramezani, C. Shi, J. Zhu, and X. Zhang, \mathcal{PT} -Symmetric acoustics, *Phys. Rev. X* **4**, 031042 (2014).
 - [11] R. Fleury, D. Sounas, and A. Alù, An invisible acoustic sensor based on parity-time symmetry, *Nat. Commun.* **6**, 5905 (2015).
 - [12] C. Shi, M. Dubois, Y. Chen, L. Cheng, H. Ramezani, Y. Wang, and X. Zhang, Accessing the exceptional points of parity-time symmetric acoustics, *Nat. Commun.* **7**, 11110 (2016).

- [13] H. Gao, H. Xue, Q. Wang, Z. Gu, T. Liu, J. Zhu, and B. Zhang, Observation of topological edge states induced solely by non-hermiticity in an acoustic crystal, *Phys. Rev. B* **101**, 180303(R) (2020).
- [14] L. Zhang *et al.*, Acoustic non-Hermitian skin effect from twisted winding topology, *Nat. Commun.* **12**, 6297 (2021).
- [15] B.-B. Wang, Y. Ge, S.-Q. Yuan, D. Jia, and H.-X. Sun, Exceptional ring by non-Hermitian sonic crystals, *Prog. Electromagn. Res.* **176**, 1 (2023).
- [16] H. Hodaei, M.-A. Miri, M. Heinrich, D. N. Christodoulides, and M. Khajavikhan, Parity-time-symmetric microring lasers, *Science* **346**, 975 (2014).
- [17] L. Feng, Z. J. Wong, R.-M. Ma, Y. Wang, and X. Zhang, Single-mode laser by parity-time symmetry breaking, *Science* **346**, 972 (2014).
- [18] A. Guo, G. J. Salamo, D. Duchesne, R. Morandotti, M. Volatier-Ravat, V. Aimez, G. A. Siviloglou, and D. N. Christodoulides, Observation of \mathcal{PT} -symmetry breaking in complex optical potentials, *Phys. Rev. Lett.* **103**, 093902 (2009).
- [19] L. Feng, Y.-L. Xu, W. S. Fegadolli, M.-H. Lu, J. E. B. Oliveira, V. R. Almeida, Y.-F. Chen, and A. Scherer, Experimental Demonstration of a unidirectional reflectionless parity-time metamaterial at optical frequencies, *Nat. Mat.* **12**, 108 (2013).
- [20] Z. Lin, H. Ramezani, T. Eichelkraut, T. Kottos, H. Cao, and D. N. Christodoulides, Unidirectional invisibility induced by \mathcal{PT} -symmetric periodic structures, *Phys. Rev. Lett.* **106**, 213901 (2011).
- [21] R. Uzdin, A. Mailybaev, and N. Moiseyev, On the observability and asymmetry of adiabatic state flips generated by exceptional points, *J. Phys. A* **44**, 435302 (2011).
- [22] G. Nenciu and G. Rasche, On the adiabatic theorem for non-self-adjoint Hamiltonians, *J. Phys. A* **25**, 5741 (1992).
- [23] J. Doppler, A. A. Mailybaev, J. Böhm, U. Kuhl, A. Girschik, F. Libisch, T. J. Milburn, P. Rabl, N. Moiseyev, and S. Rotter, Dynamically encircling an exceptional point for asymmetric mode switching, *Nature (London)* **537**, 76 (2016).
- [24] A. U. Hassan, B. Zhen, M. Soljačić, M. Khajavikhan, and D. N. Christodoulides, Dynamically encircling exceptional points: Exact evolution and polarization state conversion, *Phys. Rev. Lett.* **118**, 093002 (2017).
- [25] X.-L. Zhang, T. Jiang, and C. T. Chan, Dynamically encircling an exceptional point in anti-parity-time symmetric systems: Asymmetric mode switching for symmetry-broken modes, *Light Sci. Appl.* **8**, 88 (2019).
- [26] X.-L. Zhang, J.-F. Song, C. T. Chan, and H.-B. Sun, Distinct outcomes by dynamically encircling an exceptional point along homotopic Loops, *Phys. Rev. A* **99**, 063831 (2019).
- [27] Q. Liu, S. Li, B. Wang, S. Ke, C. Qin, K. Wang, W. Liu, D. Gao, P. Berini, and P. Lu, Efficient mode transfer on a compact silicon chip by encircling moving exceptional points, *Phys. Rev. Lett.* **124**, 153903 (2020).
- [28] X.-L. Zhang, S. Wang, B. Hou, and C. T. Chan, Dynamically encircling exceptional points: *in situ* control of encircling loops and the role of the starting point, *Phys. Rev. X* **8**, 021066 (2018).
- [29] X. Shu, A. Li, G. Hu, J. Wang, A. Alù, and L. Chen, Fast encircling of an exceptional point for highly efficient and compact chiral mode converters, *Nat. Commun.* **13**, 2123 (2022).
- [30] J. W. Yoon *et al.*, Time-asymmetric loop around an exceptional point over the full optical communications band, *Nature (London)* **562**, 86 (2018).
- [31] W. Liu, Y. Wu, C.-K. Duan, X. Rong, and J. Du, Dynamically encircling an exceptional point in a real quantum system, *Phys. Rev. Lett.* **126**, 170506 (2021).
- [32] Y. Choi, C. Hahn, J. W. Yoon, S. H. Song, and P. Berini, Extremely broadband, on-chip optical nonreciprocity enabled by mimicking nonlinear anti-adiabatic quantum jumps near exceptional points, *Nat. Commun.* **8**, 14154 (2017).
- [33] A. Li *et al.*, Hamiltonian hopping for efficient chiral mode switching in encircling exceptional points, *Phys. Rev. Lett.* **125**, 187403 (2020).
- [34] H. Nasari, G. Lopez-Galmiche, H. E. Lopez-Aviles, A. Schumer, A. U. Hassan, Q. Zhong, S. Rotter, P. LiKamWa, D. N. Christodoulides, and M. Khajavikhan, Observation of chiral state transfer without encircling an exceptional point, *Nature (London)* **605**, 256 (2022).
- [35] T. Schmiedl and U. Seifert, Efficiency at maximum power: an analytically solvable model for stochastic heat engines, *Europhys. Lett.* **81**, 20003 (2008).
- [36] S. Iram *et al.*, Controlling the speed and trajectory of evolution with counteradiabatic driving, *Nat. Phys.* **17**, 135 (2021).
- [37] See Supplemental Material at <http://link.aps.org/supplemental/10.1103/PhysRevB.110.064308> for details on derivations, algorithm and related supporting parts for the main content.
- [38] D. Guéry-Odelin, A. Ruschhaupt, A. Kiely, E. Torrontegui, S. Martínez-Garaot, and J. G. Muga, Shortcuts to adiabaticity: Concepts, methods, and applications, *Rev. Mod. Phys.* **91**, 045001 (2019).
- [39] A. P. Peirce, M. A. Dahleh, and H. Rabitz, Optimal control of quantum-mechanical systems: Existence, numerical approximation, and applications, *Phys. Rev. A* **37**, 4950 (1988).
- [40] U. Boscaïn, M. Sigalotti, and D. Sugny, Introduction to the pontryagin maximum principle for quantum optimal control, *PRX Quantum* **2**, 030203 (2021).
- [41] P. Lewalle and K. B. Whaley, Pontryagin-optimal control of a non-Hermitian qubit, *Phys. Rev. A* **107**, 022216 (2023).
- [42] M. Mitchell, *An Introduction to Genetic Algorithms* (MIT Press, Cambridge, MA, 1998).
- [43] P. T. Boggs and J. W. Tolle, Sequential quadratic programming, *Acta Numer.* **4**, 1 (1995).
- [44] A. U. Hassan, G. L. Galmiche, G. Harari, P. LiKamWa, M. Khajavikhan, M. Segev, and D. N. Christodoulides, Chiral state conversion without encircling an exceptional point, *Phys. Rev. A* **96**, 052129 (2017).
- [45] Z. X. Chen, L. L. Ma, S. J. Ge, Z.-G. Chen, M. H. Lu, Y. F. Chen, and Y. Q. Lu, Transient logic operations in acoustics through dynamic modulation, *Phys. Rev. Appl.* **21**, L011001 (2024).
- [46] J.-T. Bu *et al.*, Enhancement of quantum heat engine by encircling a liouvillian exceptional point, *Phys. Rev. Lett.* **130**, 110402 (2023).